

Quantum information processing and precise optical measurement with entangled-photon pairs

A. V. SERGIENKO and G. S. JAEGER

Two photons in a pair generated in the nonlinear optical process of spontaneous parametric down-conversion are, in general, strongly quantum entangled. Accordingly, they contain extremely strong energy, time, polarization and momentum quantum correlations. This entanglement involves more than one quantum variable and has served as a powerful tool in fundamental studies of quantum theory. It is now playing a large role in the development of novel information processing techniques and new optical measurement technologies. Here we review some of these technologies and their origins.

1. Introduction

Entangled photons allow one to carry out quantum mechanical information processing and precise optical measurements with novel characteristics. The nonlinear optical process of spontaneous parametric down-conversion, which arises in a nonlinear optical medium such as a beta-barium borate (BBO) crystal when pumped by laser light, produces entangled photons in the required quantum states. These states are those in which photons are created with strongly correlated properties that remain correlated even after the photons have propagated to widely separated locations in space [1–3]. These strong quantum correlations naturally present between down-conversion photons allow for uniquely quantum mechanical, often superior, forms of measurement to be performed. These quantum states are also capable of encoding information, with robust coherence properties associated with entanglement that allow this information to be transported and transformed in unique ways. Their resistance to the decoherence phenomena, which have hampered other approaches to quantum information processing, has put entangled-photon optics in a position of added importance. Practical technological applications can often benefit from the fact that in these states, although each individual subsystem may exhibit inherent uncertainties, the compo-

nents of the entangled pair may exhibit no such uncertainty relative to one another. This beneficial property of quantum entanglement for the development of new forms of optical measurement has given rise to the new field of quantum optical metrology.

Entangled states have been used effectively during the last two decades to carry out research demonstrating quantum efficiency measurements [4], non-local dispersion cancellation [5], entangled-photon-induced transparency [6] and entangled-photon spectroscopy with monochromatic light [7]. The practical availability of entangled beams has also made it possible to conduct experiments without having to resort to costly, rare devices. We discuss here a new generation of recently developed techniques for quantum information processing and quantum metrology.

Entangled photons first became of great interest in probing the foundations of quantum mechanics. Debates surrounding the foundations of quantum mechanics have been ongoing since the introduction of the theory, particularly since the 1930s, with entangled-photon states often playing a central role in providing essential empirical information about the quantum world. Entangled states of increasingly better quality have continually been sought in order to progressively better differentiate quantum behaviour from classical phenomena. Entangled quantum systems are defined as those quantum systems composed of at least two component subsystems which are described by states that cannot be written as a product of independent subsystem states,

Authors' addresses: Quantum Imaging Laboratory, Department of Electrical and Computer Engineering, Boston Univ., 8 Saint Mary's St., Boston MA 02215, USA (AVS and GSJ); Dept. of Physics, Boston Univ., 590 Commonwealth Ave., Boston MA 02215, USA (AVS).

$$|\Psi\rangle \neq |\psi_1\rangle \otimes |\psi_2\rangle, \quad (1)$$

for *any* two quantum states $|\psi_n\rangle$ of the individual subsystems. As Schrödinger [8], who first defined entanglement stated, entanglement is ‘the characteristic trait of quantum mechanics’.

The process known as spontaneous parametric down-conversion (SPDC) has become the most widely accepted method for creating such quantum states. New, high-intensity sources of SPDC have been developed over the last two decades (see, for example, [9]). Spontaneous parametric down-conversion of one photon into a pair is said to be of one of two definite types, based on the satisfaction of ‘phase-matching’ conditions of either type I or of type II, corresponding to whether the two photons of the down-conversion pair have the same polarization or orthogonal polarizations, respectively. The two photons of a pair, often arbitrarily called signal (s) and idler (i) for historical reasons, can also leave the down-converting medium either in the same direction or in different directions, known as the collinear and non-collinear cases, respectively.

The medium of down-conversion is usually some sort of birefringent crystal, for example, potassium dihydrogen phosphate (KDP), possessing a $\chi^{(2)}$ optical nonlinearity. Upon entrance to a nonlinear crystal, there is a small probability (on the order of 10^{-7}) that a given photon from the incident pump beam will be down-converted into a photon pair (see figure 1). If down-conversion occurs, the conserved quantities, energy and momentum, are carried into the resulting photon pair under the constraints of their respective conservation laws, with the result that the phases of the corresponding wave-functions match, in accordance with the relations

$$\omega_s + \omega_i = \omega_p, \quad k_s + k_i = k_p, \quad (2)$$

referred to as the phase-matching conditions, where the k_i and ω_i are momenta and frequencies for the three waves involved. When the two photons of a pair have different momenta or energies, entanglement will arise in SPDC, provided that the alternatives are in principle experimentally indistinguishable.

The state describing photon pairs produced in type-I down-conversion can be written

$$|\Psi\rangle = \sum_{s,i} \delta(\omega_s + \omega_i - \omega_p) \delta(k_s + k_i - k_p) |k_s\rangle \otimes |k_i\rangle. \quad (3)$$

In this case, by definition, the two photons leave the nonlinear medium with the same polarization, namely that orthogonal to the polarization of the pump beam photons. Down-conversion photons are produced in two thick spectral cones, one for each photon, within which two-photons appear each as a pair of photons on opposite sides of the pump-beam direction (see figure 1).

Entanglement between two particles in one particular quantum variable, such as spin, for example

$$|\Psi\rangle = \frac{1}{\sqrt{2}} (|\uparrow\rangle|\downarrow\rangle - |\downarrow\rangle|\uparrow\rangle), \quad (4)$$

was discussed by David Bohm in his famous book of the 1950s, *Quantum Theory* [10], and analysed by Bohm and Aharonov [11]. The nonlinear process of SPDC provides a more rich source of entanglement, instead involving several quantum variables, such as frequency, momentum, wave-vector and polarization [12].

In the mid-1980s, Hong *et al.* [13] created non-collinear, type-I phase-matched SPDC photon pairs in KDP crystal using an ultraviolet continuous-wave (cw) laser pump

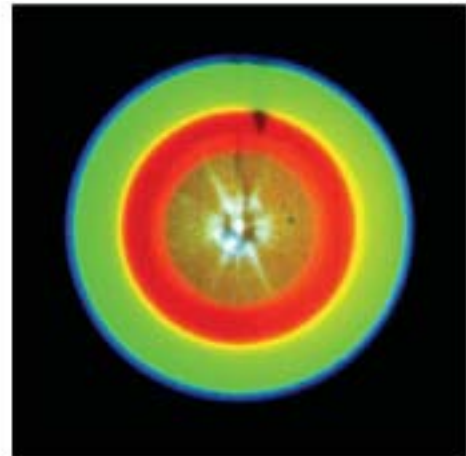
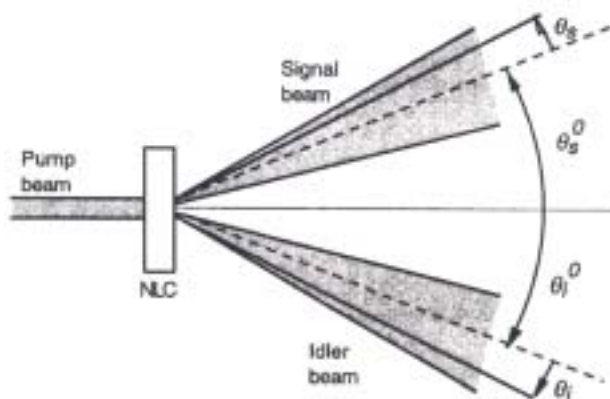


Figure 1. Spontaneous parametric down-conversion (SPDC). Here a pump laser beam strikes a nonlinear optical crystal possessing a second-order optical nonlinearity. Pairs of different colour (energy) photons emerge on the opposite sides of the pump laser forming two beams in entangled quantum states, which are cylindrically symmetrical relative to the pump direction. The central spot on the photograph is a residual pump radiation after the laser beam stop.

beam. This seminal experiment empirically demonstrated the strong temporal correlation between the two photons of a down-conversion pair. Filters were placed in the apparatus, restricting the frequency spread of the down-converted photons allowed to interfere. Note that since this experiment used type-I down-conversion, where the polarizations of the two photons are identical, there is no chance for the state entanglement to involve the polarization variable.

Since this experiment, the common approach to quantum interferometry has been to choose a single entangled parameter of interest and eliminate the dependence of the quantum state on all other parameters. For example, when investigating polarization entanglement, both strong spectral and spatial filtering are typically imposed in an attempt to restrict attention to polarization alone. A more general approach to this problem is to consider and exploit the multi-faceted nature of down-conversion photon entanglement from the outset. In such an approach, the observed quantum-interference pattern in one parameter, such as polarization, can be modified by controlling the dependence of the state on the other parameters, such as frequency and transverse wave-vector. A more complete theory of spontaneous parametric down-conversion allows us to understand the full character of fourth-order quantum interference in many valuable experiments [12]. SPDC gives rise to a quantum state that is generally entangled in three-dimensional wave-vector, energy and polarization. This means that consideration of only part of the wavefunction, such as the polarization function alone, is insufficient to capture all the quantum correlations present in the system.

Many experiments designed to verify the non-factorizability of classes of quantum states that defines entanglement are carried out in the context of models that fail to consider the overall relevant Hilbert space and are restricted to entanglement of only a single aspect of the quantum state, such as energy [14], momentum [15], or polarization [16]. Indeed, inconsistencies can emerge in the analysis of quantum-interferometric experiments involving down-conversion under such circumstances. This fact has been underlined by the failure of the conventional theory of ultrafast (femtosecond time-scale) parametric down-conversion to characterize quantum-interference experiments because femtosecond SPDC models have traditionally ignored transverse wave-vector components and have thereby not accounted for the previously demonstrated angular spread [17] of such down-converted light [18, 19]. Our techniques involve the use of these several variables and can benefit from their entanglement as our understanding of the relevant quantum states evolves yet further.

Several practical applications become available when one has the ability to efficiently produce entangled states of light. Such states have been used with great effectiveness

during the last twenty years for carrying out definitive experiments. Although each individual subsystem of an entangled system exhibits inherent uncertainty, the elements of the entangled pair may exhibit no such uncertainty relative to one another. For example, the time of arrival of an individual particle may be totally random but the two photons of an entangled pair produced in down-conversion that follow the same path always arrive simultaneously. Quantum correlations between photons generated in SPDC are not diminished by arbitrary separations between them during propagation, even when lying outside one another's light cone, allowing for what has been referred to as 'passion at a distance' [3]. It has been found that the interferometers developed for this purpose can exploit this robustness of entanglement over distance for the purposes of quantum communications, in particular for quantum cryptography [20–23].

The uniquely quantum correlations present in two-photon entangled states have opened up new realms of communications and information processing, and high-accuracy and absolute optical metrology. Research during the last two decades has produced several new technologies: (1) quantum cryptography; (2) a technique for determining polarization mode dispersion (PMD) with attosecond precision; (3) a method of absolute ellipsometry, which requires neither source nor detector calibration, nor a reference sample; (4) a novel quantum-optical optical coherence tomography technique. Quantum cryptography is a method of sending cryptographic key material under conditions of physical, rather than merely computational security. Attosecond-resolution PMD measurements provide unprecedented accuracy in determining that property which is a fundamental characteristic of optical fibres for telecommunications. Absolute ellipsometry allows one to measure the thickness and optical constants of thin films, such as semiconductors, without the need for reference samples. Quantum optical coherence tomography provides a new and potentially superior technique for the probing of volumes, providing information about their internal structure. We will now discuss each of these techniques in detail.

2. Quantum cryptography

Quantum cryptography has been based on two major techniques for quantum key distribution (QKD), both of which utilize the quantum state of the photon [20]. One approach makes use of approximately single-photon states prepared from light in a coherent state and has one major drawback: the presences of statistical fluctuations in the number of photons in the original coherent state. This adds the possibility of having two identical (unentangled) photons simultaneously in the communication channel, allowing an eavesdropper to use one photon to extract

partial information while the second proceeds to the receiver unaffected [20]. The other approach is based on the non-local character of two-photon entangled (EPR) states generated in the nonlinear process of spontaneous parametric conversion (SPDC). The unique correlation of entangled photon pairs in space, time, energy and momentum resolves the problem of the first approach. Until recently, the applicability of the latter technique has been severely limited due to the low visibility and poor system stability inherent in the use of type-I SPDC in the past, and the need for the synchronous manipulation of two Mach–Zehnder interferometers which are well separated in space, as have also been used. Based on our previous studies of quantum states and their practical utilization, we have found a way to take advantage of doubly entangled EPR states generated by type-II SPDC to provide a much more flexible, robust and reliable quantum apparatus for quantum key distribution.

The high contrast and stability of the fourth-order quantum interference patterns of entangled photons well coupled into a communications single-mode optical fibre, demonstrated in our initial experiments [21], promise to bring the performance of EPR-based quantum cryptography systems up to the level of the best single-photon systems. It has been shown recently that the use of high-repetition-rate femtosecond pulses significantly enhances the flux of entangled-photon pairs available for reliable and secure key distribution. The down-converted entangled pairs appear only at those well-defined times when pump pulses are present (repetition rate about 80 MHz). This provides narrow windows where coincidences can be obtained, separated by fixed time intervals during which the photon detectors can recover, thereby significantly enhancing the overall coincidence rate.

The key feature of quantum cryptography, the impossibility of extracting information without destroying it, cannot be exploited without suffering from a limitation on the distance of secure information transfer arising from unavoidable losses due to photon absorption in realistic quantum channels. As a matter of principle, it is impossible to amplify the quantum state, since amplification itself (cloning) requires the extraction of quantum information [24]. As a result, resource-consuming quantum error correction techniques and entanglement concentration methods are often required. The level of signal attenuation in modern optical fibres currently poses a limit of 60–75 km for reliable quantum cryptography. Open-air communication may be more feasible especially when fibres are not available (as in ship-to-ship, or in-field communication). The problem of secure communication to a satellite is also one of the most vital issues in modern telecommunication. Open-air quantum cryptography will become a crucial tool in these situations. Our technique, described below, can be realized in either manner.

The two experimental approaches to quantum cryptosystems, those that rely on weak coherent single-photon states to distribute cryptographic key bits and those that instead rely on multi-particle entanglement, can be readily compared. The weak coherent schemes are based on the protocols developed by Bennett and Brassard [25]. In these schemes, one party prepares a single-photon state by attenuating a pulsed laser to obtain a photon count of roughly 0.1 photons per pulse. The entanglement scheme developed by Ekert [26] instead involves the creation of a maximally entangled two-photon state (EPR state) and the measurement of the two particles by spatially distant parties.

There are specific advantages to using entangled states for QKD. In weak-coherent-state QKD, a laser pulse train with randomly distributed photon occupation is attenuated to achieve a high probability of 0 or 1 photons per transmitted pulse. In determining the attenuation, there is a trade-off between the shared key-bits per second and the probability that a transmitted pulse may contain more than a single photon. Since a multiple-photon pulse is vulnerable to undetected monitoring (for example, by the use of a beam splitter), the attenuation is usually increased until the probability of two photons is on the order of 0.01. This has the effect that one in ten pulses transmitted by the attenuator has a photon, reducing the possible communication rate by an order of magnitude. By contrast, in EPR QKD, each photon created and measured is accompanied by exactly one other perfectly synchronized photon, preventing any attempts at undetected beam-splitting. Furthermore, in EPR QKD the detector at the first party is capable of activating, via an authenticated message over a public line, the detector of the second party for a short temporal window, enabling the rate of false detection to be brought down to an acceptable level, making EPR QKD ideally suited for free space transmission during daylight.

A second problem with coherent state QKD is that, since the arrival of photons at the detector of the second party is governed by a random process, the active optical elements used to create the shared key must be connected to the fibre throughout the transmission. This makes them vulnerable to probe beams injected by an eavesdropper in order to determine the classical state of lasers, polarizers and phase modulators. Since the second detector in the EPR QKD is triggered for only a short duration by the response of the first detector, the eavesdropper is unable to reliably determine the classical settings of the optical elements at the precise time of the coincident detections. It should be noted that, while EPR QKD is distinguished from weak-coherent-state QKD by its inherent security advantages, both techniques can be seen as single-photon-state preparations and measurements, since even the state of the other photon of an

EPR pair collapses immediately onto an eigenstate when the first measurement is made. Previous attempts to develop the quantum cryptography with EPR states were initiated immediately after the main idea was introduced [26]. This approach requires the use of a Franson-type interferometer [27] and has been severely limited because of the low visibility inherent in the need of synchronous manipulation of the two spatially separated Mach–Zehnder interferometers mentioned above. Type-II SPDC provides a richer tool due to the two-photon entanglement both in space–time and in spin (polarization), which are not both present in entanglement generated in type-I SPDC. The unique double entanglement of the two-photon state in type-II SPDC provides us with control of the relative position of these two photons in space–time.

In our scheme [21], polarization-entangled photons are created by sending laser light through an appropriately oriented type-II second-order nonlinear crystal such as BBO. We use a collinear configuration of type-II SPDC based on the use of a double, strongly unbalanced and distributed polarization interferometer similar to the one

we designed for the polarization mode dispersion measurement (see figure 2 and section 3 below). The photons enter two spatially separated arms via a polarization-insensitive 50/50 beam splitter (BS), allowing photons of either orthogonal linear polarization to be reflected and transmitted with equal probability. One arm contains a controllable polarization-dependent optical delay (the e-ray/o-ray loop) that is required for the initial alignment of the apparatus. The introduction of polarization analysers oriented at 45° in front of each photon-counting detector completes the polarization interferometer. Signal correlation is registered by detecting the coincidence counts between the two detectors as a function of the polarization delay and of polarization angle. A phase shift imposed on one of the entangled photons does work for both of them, even though they are well separated in space. The 90° shift of the phase in one of the analysers will change the quantum interference immediately to be constructive in the central fringe with a very high (roughly 99%) contrast. The results for the Bell inequality tests using raw key-bit transmission shown in figure 3 demonstrate that the use of a polarization intensity interferometer and type-II SPDC,

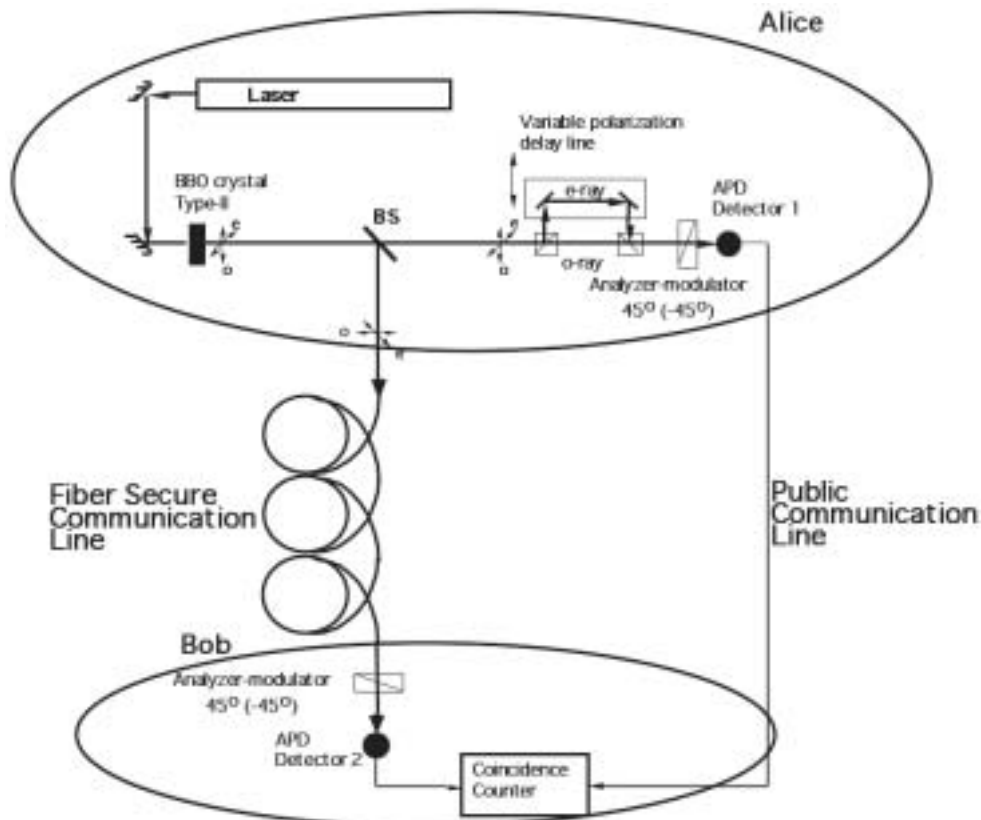


Figure 2. Entangled-photon quantum key distribution scheme [21]. Entangled photons are produced by spontaneous parametric down-conversion (see figure 1) in a collinear configuration (same direction), strike a beam splitter and reach two photon detectors (APDs) where they are measured in coincidence after passing an appropriately oriented polarization analyser. Counts at the two distant detectors are random but correlated, providing a shared, secret cryptographic key.

in contrast to spatial interferometers in type-I SPDC, provides much higher rates and contrast (visibility of quantum interference).

The final element of the procedure of quantum key distribution using this design is to randomly modulate polarization parameters of the two-photon entangled state

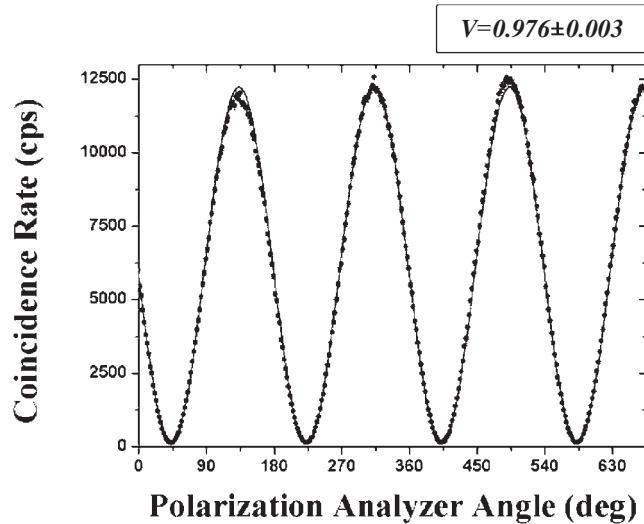


Figure 3. High visibility quantum polarization interference for quantum key bit transmission with entangled states. The solid curve is a cosine fit to evaluate the visibility of modulation.

by switching each analyser-modulator between two sets of polarization settings $0^\circ/90^\circ$ or $45^\circ/135^\circ$. This can be accomplished using fast Pockels cell polarization rotators in front of detectors. Alternatively, one can implement a passive choice of basis by introducing a pair of detector suites for each of the photons, preceded by an ordinary beam splitter that randomly sends photons to one of these two detector suites which accept polarizations in the two different polarization bases, with each photon polarization state finally distinguished by a polarizing beam splitter followed by a pair of detectors. Using a public communication line, one then can proceed with one of the standard quantum cryptography protocols described in the literature [25, 26]. The phase-sensitive quantum interference of two entangled photons in a strongly unbalanced polarization intensity interferometer delivers robust quantum hardware suitable for practical quantum cryptography applications. The high contrast and stability of quantum interference demonstrated in our experiments surpasses the performance of the best single-photon polarization techniques, without the limitations outlined above.

3. Quantum metrology: measurement of polarization mode dispersion

Conventional polarization measurement techniques were developed over the years to a very high degree of

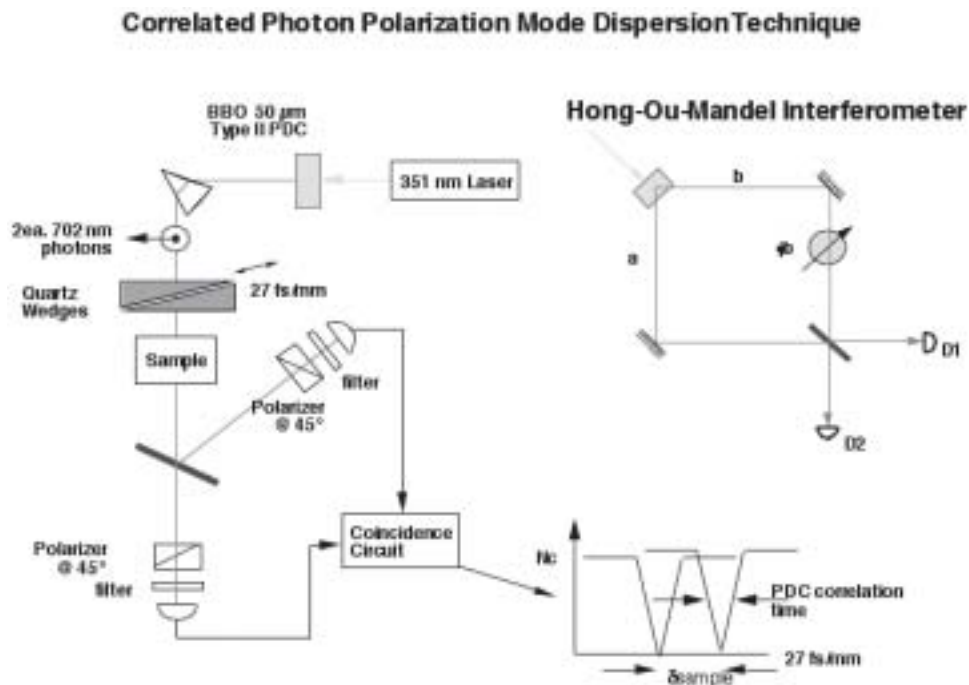


Figure 4. Schematic of a two-photon polarization interferometer in comparison with its traditional analogue, the Hong–Ou–Mandel intensity interferometer (top right). This interferometric dip (lower right) is shifted proportional to the temporal delay introduced by polarization mode dispersion in the sample under measurement [28].

performance and are used every day in many research and industrial applications. Traditional, non-polarization-based techniques for the measurement of optical delay usually make use of monochromatic light. The introduction of an optical sample in one arm of the interferometer causes a sudden shift of interference pattern

(sometimes over tens or hundreds of wavelengths) proportional to the absolute value of the optical delay. This approach requires one to keep track of the total number of shifted interference fringes in order to evaluate the absolute value of the optical delay. The accuracy of this approach is limited by the stability of the inter-

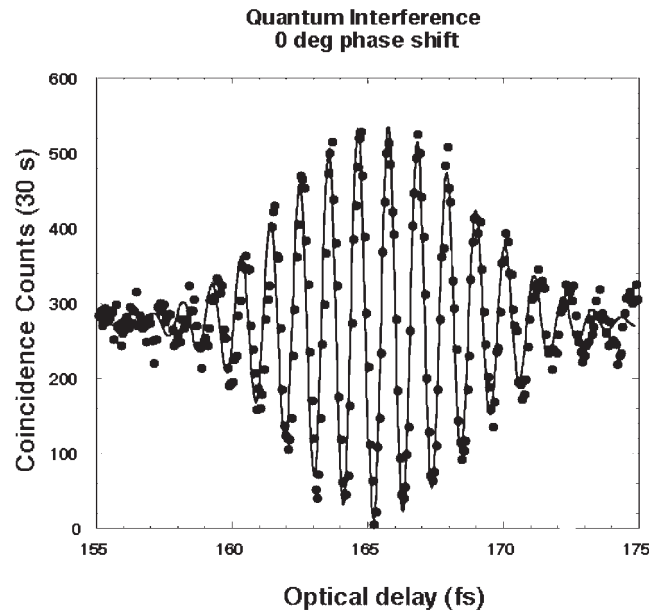
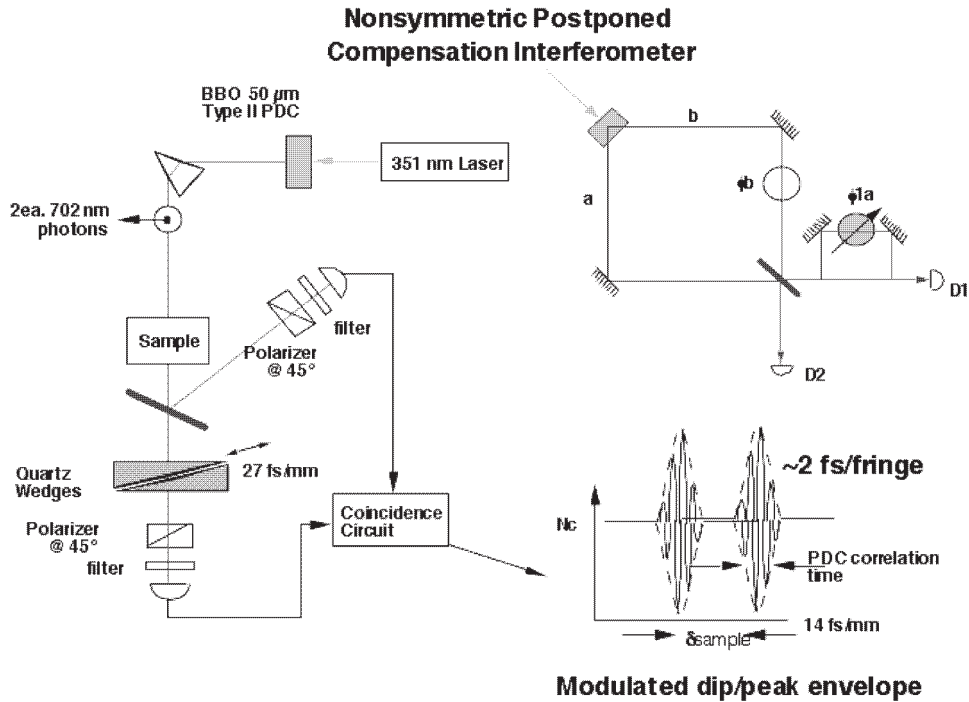


Figure 5. (a) Schematic of a two-photon polarization interferometer with a postponed optical delay. A non-symmetric delay is introduced only in one arm after the beam splitter. (b) Measurement of intensity correlations as a function of relative femtosecond polarization delay τ . Note that the V-shaped feature is modulated in this arrangement [29].

ferometer, the signal-to-noise level of the detector and the wavelength of the monochromatic radiation used. Conventional polarization interferometers used in ellipsometry measurements provide very high resolution but have a similar problem of tracking the absolute number of 2π shifts of optical phase during the polarization mode dispersion measurement.

Optical engineers have come up with several ways to get around this problem, using additional complex measurement procedures. The use of monochromatic classical polarized light does not allow one to measure the relative delay between two orthogonal waves in a single measurement, so several measurements at different frequencies must be used to reconstruct the polarization dispersion properties of materials. The use of highly monochromatic laser sources creates the additional problem of multiple reflections and strong irregular optical interference, especially in studying surface effects. Ellipsometry with low-coherence sources (white light) has received attention as a convenient method for the evaluation of dispersions in optical materials, particularly of communication fibres. While the technique provides the high timing resolution, along with the absolute nature of the optical delay measurement, it

suffers from the problem of low visibility and instability of the interference pattern.

The unique double entanglement of the two-photon state in type-II phase-matched SPDC again provides us with ultimate control of the relative position of photon pairs in space–time, providing a way of avoiding the limitations of conventional techniques. The study of polarization entanglement and of the natural rectangular shape of the two-photon wave function in space–time in type-II phase-matched SPDC allows us to measure propagation time delay in optical materials with sub-femtosecond resolution. This entangled photon state intrinsically provides an absolute value for polarization optical delay that is not limited to producing only a value relative to one wave cycle of light as is the case in conventional methods. The probe light does not disturb the physical conditions of the sample under test, and can be used continuously during the growth and assembly processes to monitor major optical parameters of the device *in situ*. By manipulating the optical delay between the orthogonally polarized photons, a V-shaped correlation function feature is realized by a coincidence photon counting measurement [28]. The general principle and

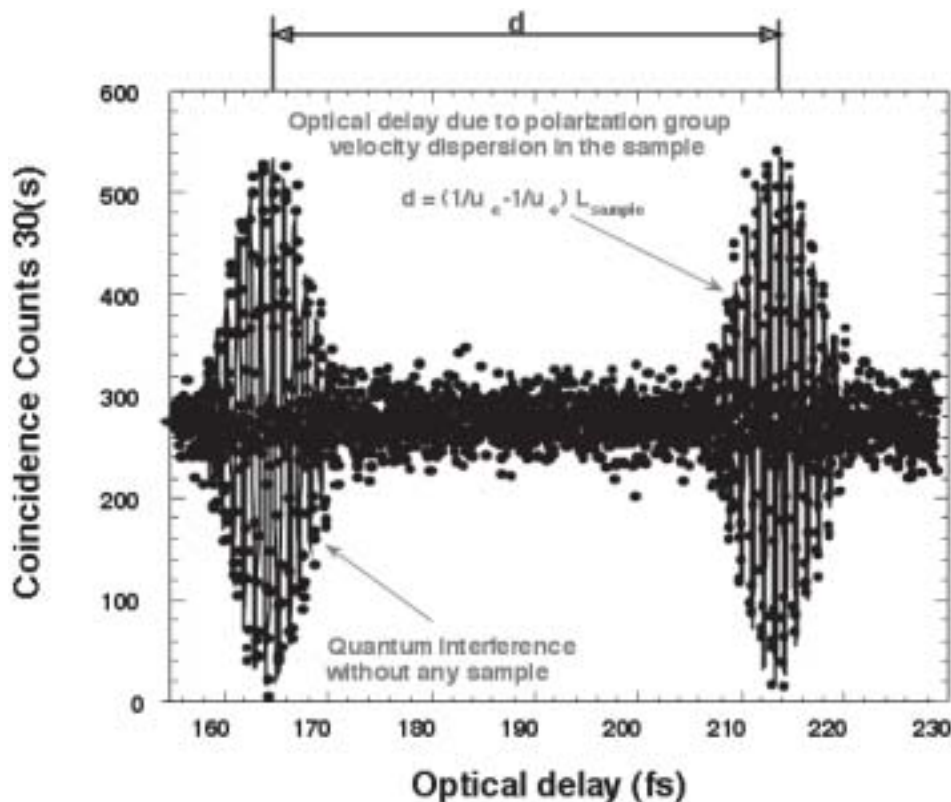


Figure 6. Measurement of the optical delay in the crystal quartz sample using a $50 \mu\text{m}$ nonlinear crystal for SPDC [29]. The horizontal scale is the femtosecond polarization time delay τ introduced by the variable-thickness birefringent optical device located after the beam splitter, BS.

schematic experimental set-up is illustrated in figure 5. The sharp V in the intensity correlation function can be made just 5–10 fs wide. The introduction of any additional sample of optical material or photonic device with different group velocities for o-rays, (u_o) than for e-rays, (u_e) in the optical path before the beam splitter will shift the V-shape distribution on a sub-femtosecond time scale. This shift is proportional to the optical delay in the sample of the length L :

$$d = (1/u_o - 1/u_e)L \approx (n_o - n_e)L/c. \quad (5)$$

In our realization, a 351 nm Ar^+ laser pumps the BBO crystal in a collinear and frequency-degenerate configuration. Pairs of orthogonally polarized photons generated in the BBO nonlinear crystal enter two spatially separated arms via a polarization-insensitive 50/50 beam splitter (BS), so both ordinary and extraordinary polarized photons have equal probability to be reflected and transmitted. The two analysers (oriented at 45°) in front of each photon-counting detector D1 (D2) complete the creation of what are, in essence, two spatially separated polarization interferometers for the originally X (Y)-oriented signal and idler photons. Signal correlation is registered by coincidence events between detectors D1 and D2, as a function of a variable polarization delay (PD) in the interferometer. Spontaneous parametric down-conversion in a BBO nonlinear crystal with $L = 0.05$ to 1 mm generates signal and idler photons with coherence lengths of tens to hundreds of femtoseconds. This approach explicitly utilizes a self-referencing feature of (polarization) entangled states discussed earlier.

A very useful new feature is realized in our experiment due to the non-symmetric manipulation of the relative optical delay τ between ordinary and extraordinary photons in only one of the two spatially separated interferometers. Namely, the observed coincidence probability interferogram has its triangular envelope now filled with an almost 100% modulation, which is associated with the period of pump radiation. The additional introduction of a sample of optical or photonic material with different o-ray and e-ray group velocities in the optical path before the beam splitter shifts the interference pattern proportional to $\tau_{\text{sample}} = d/c$, the difference in propagation times of the two polarizations. This allows one to measure directly the absolute value of total optical delay between two orthogonally polarized waves in the sample on a very fine, sub-femtosecond time scale [28, 29].

The observed result of the measurement of intensity correlations, corresponding to the coincidence probability, as a function of relative polarization delay d , is illustrated in figure 6. The SPDC signal is delivered to the detectors without the use of any limiting spectral filters. The full width at half-maximum (FWHM) of the correlation function envelope is defined by

$$\delta = (1/u_o - 1/u_e)L_{\text{crystal}}. \quad (6)$$

The high visibility of the interference pattern and the extremely high stability of the polarization interferometer in such a collinear configuration allows one to identify the absolute shift of the wide envelope with an accuracy defined by the fringe size of an internal modulation.

It is important to note the high contrast of observed quantum interference, approximately 90%. The resolution is further enhanced by reducing the total width of the envelope [28]. This can be done by widening the phase matching spectrum by reducing the crystal length to $50 \mu\text{m}$. This arrangement was used to measure the optical delay of a quartz sample introduced into the optical path before the beam splitter BS. The result of this measurement (performed with the $50 \mu\text{m}$ nonlinear crystal) is illustrated in figure 6. The 10 fs width of the envelope enables us to clearly identify the central fringe position. Based on our signal-to-noise ratio, we expect to resolve at least 1/100 of a fringe about (10^{-17} s).

This technique for linear polarization dispersion measurement is easily convertible to the case of circular polarization. All advantages of using quantum correlation remain intact. This technique is also easily modified to study optical interactions at the surfaces of materials. To do this we exploit a reflection configuration, rather than the transmission configuration, and take advantage of the strong polarization dependence of evanescent waves. This approach is a uniquely sensitive tool for the analysis of the orientation, structure, morphology and optical properties of single and multiple layers of atoms, either grown or deposited on a substrate. The technique may also be sensitive to the chemical identity of adsorbed molecules and atoms, in which case it would be applicable for use in chemical sensors.

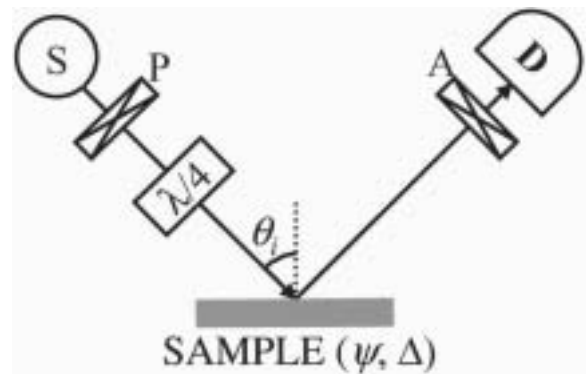


Figure 7. The null ellipsometer. S is an optical source, P is a linear polarizer, $\lambda/4$ is a quarter-wave plate (compensator), A is a linear polarization analyser and D is an optical detector; θ_i is the angle of incidence. The sample is characterized by the ellipsometric parameters ψ and Δ [31].

4. Quantum ellipsometry

Ellipsometry [30–35] is a well-known metrological technique used to determine the thickness and optical constants of thin-film samples, especially in the semiconductor industry. One important example of the application of ellipsometric techniques is their use in non-destructive measurements of the film thicknesses of layers used for gate isolation in integrated circuits. As the dimensions of the components used for integrated circuits decrease, the thicknesses of these isolating layers also needs to be decreased [36]. The accuracy of these measurements is increasingly important for process control. A thin film can be characterized by two parameters, ψ and Δ : ψ is related to the magnitude of the ratio of the eigen-polarization complex reflection coefficients of the sample, \tilde{r}_1 and \tilde{r}_2 , via $\tan \psi = |\tilde{r}_1/\tilde{r}_2|$ and Δ is the phase shift between them [31].

The high accuracy required in traditional ellipsometric measurements necessitates the absolute calibration of both the source and the detector. Ellipsometry makes use of a myriad of experimental techniques for circumventing the imperfections of the devices involved. The most common techniques are null and interferometric ellipsometry. Both techniques suffer the drawback of requiring a reference sample for calibration prior to inserting the sample of interest.

In the traditional null ellipsometer [31], depicted in figure 7, the sample is illuminated with a beam of light that can be prepared in any polarization state. The reflected light, generally in an elliptically polarized state, is then analysed. The polarization of the incident beam is adjusted to compensate for the change in the relative amplitude and phase between the two eigen-polarizations induced by the sample, so that the reflected beam is linearly polarized. If passed through an orthogonal linear polarizer, this beam will yield a null (zero) measurement at the optical detector. The null ellipsometer does not require a calibrated detector since it does not measure intensity, but instead records a null. The principal drawback of null measurement techniques is the need for a reference to calibrate the null. This is needed, for example, to find its initial location (the rotational axis of reference at which an initial null is obtained) for comparison with the subsequent location after inserting the sample into the apparatus. Such a technique alleviates the problem of an unreliable source and detector, but necessitates the use of a reference sample. The accuracy and reliability of all measurements depend on previous knowledge of the parameters of this reference sample. In this case, the measurements are a function of ψ , Δ and the parameters of the reference sample.

Another possibility is to perform a type of ellipsometry that employs an interferometric configuration, in which the light from the source follows more than one path, usually created via beam splitters, before reaching the detector. The sample is placed in one of those paths. Assuming that the

source is reliable, one can then estimate the efficiency of the detector by performing measurements when the sample is removed. Although this configuration alleviates the problem of an unreliable detector, it depends on the reliability of the source and suffers from the drawback of requiring several optical components (beam splitters, mirrors, etc.). The ellipsometric measurements are a function of ψ , Δ , source intensity and the parameters of the optical elements. The accuracy of the measurements is therefore limited by knowledge of the parameters characterizing these optical components, necessitating the use of a reference sample. The stability of the optical arrangement is also of importance to the performance of such a device.

Standard reference materials, such as thermal oxide on silicon, offered by the National Institute of Standards & Technology (NIST), yield certified values of Δ and ψ for specific angles of incidence and at a specific wavelength (usually 632.8 nm). This means that for any other angle of incidence or wavelength used, reliable values of Δ and ψ cannot be provided. Furthermore, even at the specified angle of incidence and wavelength, ψ and Δ are only as accurate as the technique used to determine them, which must rely on the use of some other reference. Recently, work has been carried out on manufacturing reference materials for which ψ is an insensitive parameter around specific angles of incidence [37]. Although these new reference materials promise improvements, the ellipsometric parameters are still not certified over the entire range of angles of incidence. Furthermore, the certification data provided with standard reference materials are based on the assumption that one has a fully working ellipsometer in error-free operation. NIST only guarantees, provided one has well-characterized polarizers and optical components, the exact wavelength of choice and the exact angle of incidence of interest, that the reference material will yield the expected values of ψ and Δ . A major problem is that one cannot separate errors arising from the ellipsometer from those associated with the reference material.

Another issue of concern with standard reference materials is that their utility is limited when used outside their specified tolerances. For example, standard reference materials that are semiconductors become oxidized with time, and so must be considered as three-phase (ambient–thin film–substrate) systems rather than two-phase systems as when new. Some of these oxides have been shown to exhibit small variations in thickness over the full wafer, leading to disagreements with the assumed model. Some have used hydrogen-terminated single-crystal silicon (Si) because its surface is said to be stable, containing no native oxides. However, this stability lasts for only a few tens of minutes [32], after which this sample can no longer be considered a reliable reference material. A surface with properties that change with time cannot be considered self-verifiable, and thus cannot be used as a reliable reference.

A novel technique for obtaining reliable ellipsometric measurements has been proposed that is based on the use of photon pairs produced by spontaneous optical parametric downconversion (SPDC) [1, 19, 38–41]. We have extended the use of this non-classical light source to the field of ellipsometry [42, 43], and demonstrated that absolute ellipsometric results can be obtained from a semiconductor sample. All classical optical sources (including ideal amplitude-stabilized lasers) suffer from unavoidable quantum fluctuations, even if all other extraneous noise sources are removed. Fluctuations in the photon number can only be eliminated by constructing a source that emits non-overlapping wave packets, each of which contains a fixed photon number. Such sources have been investigated, and indeed sub-Poisson light sources have been demonstrated [44–46]. One such source may be readily realized via SPDC from a second-order nonlinear crystal illuminated with a monochromatic laser pump [1].

Recall that, in type-II phase-matched SPDC, the signal and idler photons have orthogonal polarizations, one extraordinary and the other ordinary. These two photons emerge from the nonlinear crystal (NLC) with a relative time delay due to its birefringence [47]. Passing the pair through an appropriate birefringent material of suitable length will compensate for this time delay. Such compensation is required for extracting ψ and Δ from the measurements. When compensation is not employed one may obtain ψ , but cannot obtain Δ .

Recall also that the signal and idler in SPDC may be emitted in two different directions (the non-collinear case) or in the same direction (the collinear case). In the non-collinear case, the SPDC state is polarization entangled, with its quantum state described by [47]

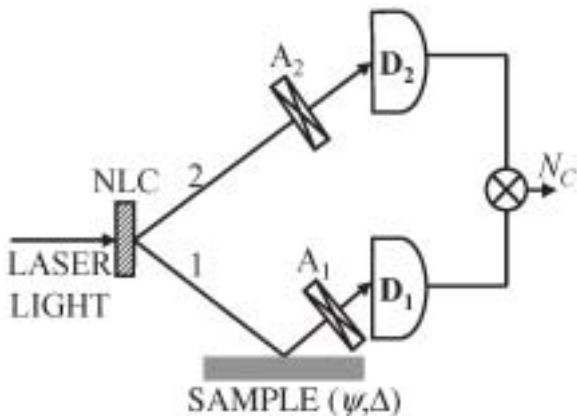


Figure 8. Polarization-entangled twin-photon ellipsometer. The quantum correlations between photons, each going to its own detector, are used in coincidence to obtain ellipsometric quantities from detector count rates [43].

$$|\Psi\rangle = \frac{1}{2^{1/2}}(|H\rangle|V\rangle + |V\rangle|H\rangle), \quad (7)$$

where $|H\rangle$ and $|V\rangle$ represent horizontal and vertical polarizations, respectively [48]. Again, it is understood that the first polarization indicated is that of the signal photon and the second is that of the idler. Such a state cannot be written as the product of states of the signal and idler photons. Although equation (7) represents a pure quantum state, the signal and idler photons considered separately are each unpolarized [49, 50]. The state represented in equation (7) assumes that there is no relative phase between single-particle (signal or idler) state vectors. Although the relative phase may be non-zero, it can usually be arbitrarily chosen by making small adjustments to the NLC. In the collinear case, the quantum state produced by down-conversion is a polarization-product state

$$|\Psi\rangle = |H\rangle|V\rangle. \quad (8)$$

Because it is factorizable (i.e. it may be written as the product of states of the signal and idler photons), this state is not entangled.

Consider now a configuration based on the use of non-collinear type-II down-conversion. Such an apparatus, referred to as the ‘entangled twin-photon ellipsometer’ [42, 43], or quantum ellipsometer, makes use of polarization-entangled photon pairs (see figure 8). An advantage of such a device over its idealized null ellipsometric counterpart is that the arms of the ellipsometer are separate and the light beams traverse them independently in different directions. This allows various instrumentation errors of the classical set-up to be avoided. For example, placing optical elements before the sample causes beam deviation errors [51] when the faces of the optical components are not exactly parallel, leading to an error in the angle of incidence and to errors in the estimated parameters. In our case, no optical components are placed between the (NLC) source and the sample, since any desired polarization manipulation can be performed in the other arm of the entangled twin-photon ellipsometer. Furthermore, one can change the angle of incidence to the sample easily and repeatedly.

It can be shown that

$$N_c = C[\tan \psi \cos^2 \theta_1 \sin^2 \theta_2 + \sin^2 \theta_1 \cos^2 \theta_2 + 2(\tan \psi)^{1/2} \cos \Delta \cos \theta_1 \cos \theta_2 \sin \theta_1 \sin \theta_2], \quad (9)$$

where the constant of proportionality C depends on the efficiencies of the detectors and the duration of accumulation of coincidences [43]. One can obtain C , ψ and Δ by setting, for example, $\theta_1 = 0^\circ$, $\theta_1 = 90^\circ$, and $\theta_1 = 45^\circ$, while θ_2 is scanned at each setting of θ_1 .

If the sample is replaced by a *perfect* mirror, the coincidence rate in equation (9) becomes a sinusoidal pattern of 100% visibility, $C \sin^2(\theta_1 + \theta_2)$, as previously

indicated. In practice, by judicious control of the apertures placed in the down-converted beams, visibilities close to 100% can be obtained. To understand the need for temporal compensation discussed previously, we re-derive equation (9), which assumes full compensation, for the case when a birefringent compensator is placed in one of the arms of the configuration:

$$N_c = C[\tan \psi \cos^2 \theta_1 \sin^2 \theta_2 + \sin^2 \theta_1 \cos^2 \theta_2 + 2(\tan \psi)^{1/2} \cos \Delta \cos \theta_1 \cos \theta_2 \sin \theta_1 \sin \theta_2 \Phi(\tau) \cos(\omega_o \tau)]. \quad (10)$$

Here τ is the birefringent delay, ω_o is half the pump frequency and $\Phi(\tau)$ is the Fourier transform of the SPDC normalized power spectrum. When $\tau = 0$ we recover equation (9), whereas when τ is larger than the inverse of the SPDC bandwidth, the third term that includes Δ becomes zero and thus Δ cannot be determined. An interesting feature of this interferometer is that it is not sensitive to an overall mismatch in the length of the two arms of the set-up, which increases the robustness of the arrangement.

An advantage of this set-up over its idealized null ellipsometric counterpart, discussed earlier, is that the two arms of the ellipsometer are separate and the light beams traverse them independently in different directions. This allows various instrumentation errors of the classical set-up to be circumvented. For example, placing optical elements before the sample causes beam deviation errors [51] when the faces of the optical components are not exactly parallel. This leads to an error in the angle of incidence and, consequently, errors in the estimated parameters. In our case, no optical components are placed between the source (NLC) and the sample; any desired polarization manipula-

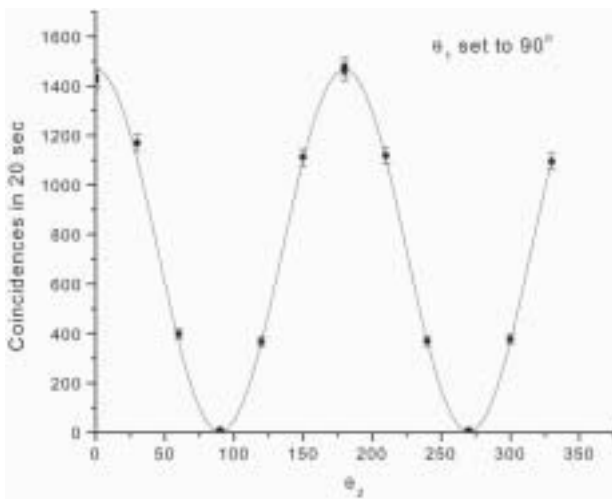


Figure 9. Coincidence interference pattern determined by scanning the angle θ_2 , with θ_1 fixed at 90° .

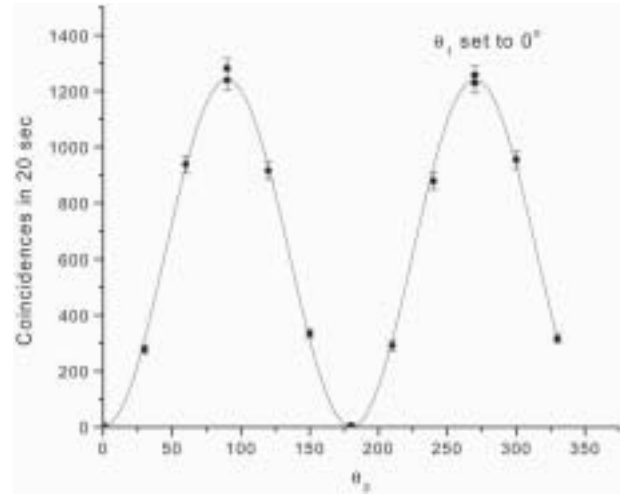


Figure 10. Coincidence interference pattern determined by scanning the angle θ_2 , with θ_1 fixed at 0° .

tion may be performed in the other arm of the entangled twin-photon ellipsometer. Furthermore, one can change the angle of incidence to the sample easily and repeatedly.

A significant limitation of classical ellipsometry is the difficulty of fully controlling the polarization of the incoming light. A linear polarizer is usually employed at the input of the ellipsometer, but the finite extinction coefficient of this polarizer causes errors in the estimated parameters [31]. In the entangled twin-photon ellipsometer, the polarization of the incoming light is dictated by the phase-matching conditions (equation (2)) of the nonlinear interaction in the nonlinear crystal. The polarizations defined by the orientation of the optical axis of the crystal play the role of the input polarization in classical ellipsometry. The crystal is aligned for type-II phase-matching, where only one polarization component of the pump generates SPDC since the orthogonal component cannot satisfy the phase-matching conditions. The advantage is that the down-conversion process assures the stability of polarization along a particular direction.

Our experiments have shown that polarization-entangled photon pairs can be used to obtain values of ψ that are comparable to those obtained from traditional ellipsometers. In our apparatus, configured shown in figure 8, a Si sample was tested at an angle of incidence of 30° . A 406 nm cw Kr^+ laser pump illuminated a BBO NLC to produce degenerate twin photons centred at 812 nm. Two avalanche photodiodes operating in the Geiger mode were used as detectors (D_1 and D_2). Interference filters centred at 810 nm with 10 nm bandwidths were placed in front of each detector.

In the initial step of the procedure, the angle of the analyser A_1 , denoted θ_1 , was set to 90° while θ_2 was scanned. The sinusoidal pattern for the coincidence rate at

this setting is shown in figure 9, which, for $\theta_1 = 90^\circ$, is described by

$$N_c = C \cos^2 \theta_2 \quad (11)$$

so the amplitude of this curve provides the value for C . In the second step of the procedure, θ_1 was set to 0° while θ_2 was again scanned. The results for the coincidences are shown in figure 10, described by

$$N_c = C[\tan \psi \sin^2 \theta_2], \quad (12)$$

so that the amplitude of this function is equal to $C \tan \psi$. One can therefore determine ψ simply by dividing the two functions. Using this approach, ψ was determined to be 40.2° for our Si sample. The expected value for ψ at this angle of incidence is 40.4° , in accordance with calculations carried out using the appropriate Sellmeier dispersion formula [52, 53].

The interference patterns obtained using a technique similar to the one described above did not provide a reasonable value for Δ , however. The main reason for this is that the expressions used to obtain ψ presumed a visibility of 100%. In order to obtain Δ , a visibility term must be included that can take a value less than 100%. Another potential source of error resides in the model used to determine the ellipsometric parameters. As mentioned above, unless specially treated, semiconductors become oxidized by air and develop thin oxide layers. The sample model must account for this thin oxide layer by considering one to have a three-phase, rather than a two-phase, system. Either model would lead to a significantly different Δ for the same sample.

We have explained that entangled twin-photon ellipsometry is self-referencing and therefore eliminates the necessity of constructing an interferometer altogether. This remarkable property is due to fourth-order (coincidence)

quantum interference of photon pairs associated with non-local polarization entanglement. Preliminary results for ψ with a silicon sample have been obtained. Our quantum ellipsometer is subject to the same shot-noise-limited, as well as angularly resolved, precision that is obtained with traditional ellipsometers (interferometric and null systems, respectively), but removes the limitation in accuracy that results from the necessity of using a reference sample as in traditional ellipsometers.

5. Quantum optical coherence tomography

Another new quantum technique, for carrying out tomographic measurements with dispersion-cancelled resolution, has been introduced, called quantum optical coherence tomography (QOCT). QOCT makes use of a two-photon interferometer in which a swept delay permits a coincidence interferogram to be traced. The use of a non-classical entangled twin-photon light source permits measurements to be made at depths greater than those accessible via ordinary, classical optical coherence tomography (OCT) which works by focusing a beam of light into materials and measuring the intensity and position of the resulting reflections and suffers from the negative effects of sample dispersion [54]. QOCT offers higher sensitivity than classical OCT and a doubling of resolution for the same source bandwidth [55]. In this case, simple type-I SPDC satisfies our correlation requirements.

The twin-photon source we use is characterized by a frequency-entangled state given by [56]

$$|\Psi\rangle = \int d\Omega \zeta(\Omega) |\omega_0 + \Omega, \omega_0 - \Omega\rangle, \quad (13)$$

where Ω is the angular frequency deviation about the central angular frequency ω_0 of the twin-photon wave packet, $\zeta(\Omega)$ is the spectral probability amplitude and the spectral distribution of the wave packet $S(\Omega) = |\zeta(\Omega)|^2$ is normalized such that $\int d\Omega S(\Omega) = 1$. For simplicity, assume S is a symmetric function and that both photons reside in a common single spatial and polarization mode. The HOM beam splitter interferometer [13] is modified by placing a reflective sample in one of the paths in the interferometer and a temporal delay τ is inserted in the other path, as shown in figure 11. The two photons, represented by beams 1 and 2, are then directed to the two input ports of a symmetric beam splitter. Beams 3 and 4, the outputs of the beam splitter, are directed to two single-photon-counting detectors, D_1 and D_2 . The coincidences of photons arriving at the two detectors are recorded within a time window determined by a coincidence circuit. The delay τ is swept and the coincidence rate $C(\tau)$ is monitored.

For a sample described by $H(\omega) \int_0^\infty dz r(z, \omega) \exp [i2\varphi(z, \omega)]$, the coincidence rate $C(\tau)$ is given by

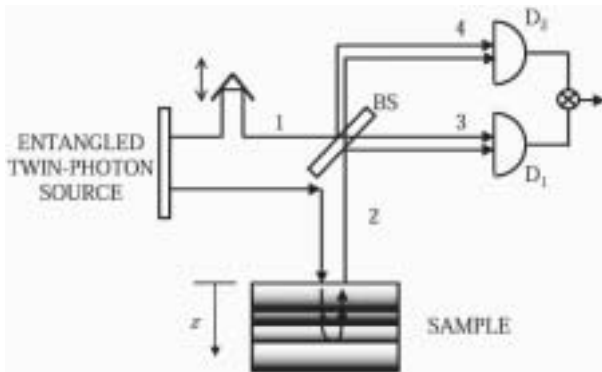


Figure 11. Set-up for quantum optical coherence tomography (QOCT). BS stands for beam splitter and τ is a temporal delay. D_1 and D_2 are single-photon-counting detectors that feed a coincidence circuit [55].

$$C(\tau) \propto \Lambda_0 - \text{Re}\{\Lambda(2\tau)\}, \quad (14)$$

where the self-interference term Λ_0 and the cross-interference term $\Lambda(\tau)$ are defined as follows:

$$\Lambda_0 = \int d\Omega |H(\omega_0 + \Omega)|^2 S(\Omega) \quad (15)$$

and

$$\begin{aligned} \Lambda(\tau) &= \int d\Omega H(\omega_0 + \Omega) H^*(\omega_0 - \Omega) S(\Omega) \exp(-i\Omega\tau) \\ &= h_q(\tau) * s(\tau), \end{aligned} \quad (16)$$

where $h_q(\tau)$ is the inverse Fourier transform of $H_q(\Omega) = H(\omega_0 + \Omega)H^*(\omega_0 - \Omega)$ with respect to Ω .

There are important differences and similarities between QOCT and OCT interferograms. The unity OCT background level in OCT is absent for QOCT, with the QOCT cross-interference term in equation (16) being related to the reflection from the sample quadratically; the sample reflection is therefore simultaneously probed at two frequencies, $\omega_0 + \Omega$ and $\omega_0 - \Omega$. Moreover, the factor of 2 by which the delay in the QOCT cross-interference term in equation (14) is scaled, in compar-

ison to that for OCT, leads to an enhancement of resolution in the former.

An idealized sample model can be used with a discrete summation in place of the continuous sum above

$$H(\omega) = \sum_j r_j(\omega) \exp[i2\phi_j(\omega)], \quad (17)$$

over the layers that constitute the sample. This is a suitable approximation for samples that are layered as many biological samples and semiconductor devices are, but not one necessary to apply the technique.

Equations (16) and (17) result in a cross-interference term given by the sum of two contributions:

$$\begin{aligned} \Lambda(\tau) &= \sum_j |r_j|^2 s\left(\tau - 4\frac{z_j}{v_0}\right) + \sum_{j \neq k} r_j r_k^* s_d^{(jk)} \\ &\quad \left(\tau - 2\frac{z_j + z_k}{v_0}\right) \exp[i2\beta_0(z_j - z_k)], \end{aligned} \quad (18)$$

where the first contribution represents reflections from each layer without group-velocity dispersion and the second contribution represents cross-terms arising from interference between reflections from each pair of layers. The quantity $s(\cdot)$ is the correlation function of

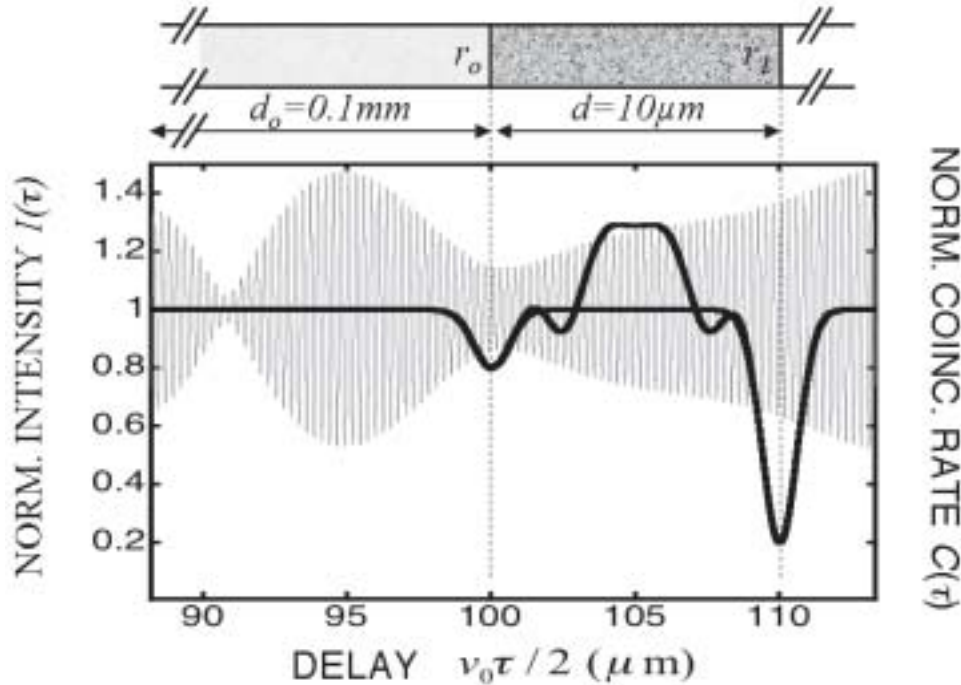


Figure 12. Normalized intensity $I(\tau)$ (thin rapidly varying grey curve and left ordinate) and normalized coincidence rate $C(\tau)$ (thick black curves and right ordinate) versus normalized delay (scaled by half the group velocity, $v_0/2$) for quantum optical coherence tomography of a two-layer sample underneath a dispersive medium. The black broken curve represents the full QOCT signal (equation (18)) whereas the black solid curve represents the QOCT signal after averaging over the pump frequency (equation (18), first contribution). The black broken curve coincides with the black solid curve everywhere except where the black broken curve can be seen. The structure of the sample is shown at the top of the figure [55].

the source defined previously and the quantity $s_d^{(jk)}(\cdot)$ is a Fresnel transformation. In contrast to OCT, only dispersion between the j th and k th layers survives, as is evident by the superscript (jk) . The terms of the first contribution in equation (18) include the information that is often sought in OCT: characterization of the depth and reflectance of the layers that constitute the sample. The terms comprising the second contribution in equation (18) are dispersed due to propagation through the inter-layer distances $z_j - z_k$ but carry further information about the sample that is inaccessible via OCT.

Consider a sample comprised of two reflective layers buried at some depth below the surface of a medium, as illustrated at the very top of figure 12. Neglecting reflection from the top surface of the sample and assuming a highly dispersive material, with the knowledge that ‘higher dispersion crown glass’ [57] is even more highly dispersive than assumed here, one obtains results of the type shown in figure 12 for OCT (thin rapidly varying grey curve) and QOCT (black broken curve representing the full signal; black solid curve representing the signal averaged over pump frequency). Due to dispersion, it is clear that no useful information about the sample is available from OCT in this realistic case. QOCT, on the other hand, yields a pair of high-resolution dispersion-cancelled coincidence-rate dips at delays corresponding to reflections from the two surfaces. Moreover, the QOCT resolution is a factor of 2 better than that achievable via OCT in a dispersion-free medium. The peak between the two dips evidenced in the full QOCT signal (black broken curve) that could alternatively be a dip, depending on the phases of the terms in the second contribution in equation (18), is the result of quantum interference between the probability amplitudes arising from reflection from the two different surfaces. This is in contrast to the black solid-curve dips, which are a result of quantum interference between the probability amplitudes arising from reflection from each surface independently. The width of the middle peak is determined only by the dispersion of the medium residing between the two reflective surfaces and not by the nature of the material under which they are buried. The dispersion of the region between the two surfaces is determined by measuring the broadening of the middle peak in comparison with the two dips.

6. Conclusion

Entangled-photon states, particularly entangled-photon pairs created by spontaneous parametric down-conversion, provide a natural basis for quantum information processing and quantum measurement due to the strong correlations between photons, even when widely separated. The interdependence of physical parameters due to entangle-

ment allows one to consider greater properties of the Hilbert space occupied by the complete entangled quantum state with its dependency on multiple variables. The strong quantum correlations naturally present between down-conversion photons allow for uniquely quantum mechanical, often superior, forms of measurement to be performed. Practical technological applications benefit from the fact that, in these states, although each individual subsystem can exhibit inherent uncertainties, the components of the entangled pair may exhibit no such uncertainty relative to one another.

Unique new forms of information encoding and manipulation and high-precision measurements can be performed using entangled quantum states providing several advantages over classical techniques. We have shown how entangled states allow quantum information to be encoded and this quantum information securely transmitted to a remote location, in a manner superior to other proposed quantum-mechanical methods. Entanglement has also allowed for the development of new forms of optical measurement, giving rise to the new field of quantum optical metrology. We showed how one is also able to exploit the correlations of entangled photons to create new metrological techniques, including polarization-mode-dispersion measurements, quantum ellipsometry and quantum optical coherence tomography, having significant advantages over their classical counterparts.

References

- [1] Klyshko, D. N., 1980, *Photons and Nonlinear Optics* (Moscow: Nauka), chaps 1 and 6 [translation: 1998 (New York: Gordon and Breach Science Publishers)].
- [2] Mandel, L., and Wolf, E., 1995, *Optical Coherence and Quantum Optics* (Cambridge: Cambridge University Press).
- [3] Shimony, A., 1993, *The Search for a Naturalistic World View*, Vol. 2 (Cambridge: Cambridge University Press), p. 133.
- [4] Penin, A. N., and Sergienko, A. V., 1991, *Appl. Opt.*, **30**, 3582.
- [5] Kwiat, G., and Chiao, R. Y., 1992, *Phys. Rev. A*, **45**, 6659.
- [6] Fei, H.-B., Jost, B. M., Popescu, S., Saleh, B. E. A., and Teich, M. C., 1997, *Phys. Rev. Lett.*, **78**, 1679.
- [7] Saleh, B. E. A., Jost, B. M., Fei, H.-B., and Teich, M. C., 1998, *Phys. Rev. A*, **57**, 3972.
- [8] Schrödinger, E., 1935, *Naturwissenschaften*, **23**, 807; 1935, *ibid.*, **23**, 823; 1935, *ibid.*, **23**, 844 [translation: Trimmer, J. D., 1980, *Proc. Am. phil. Soc.*, **124**, 323; reprinted in Wheeler, J. A., and Zurek, W. H. (eds), 1983, *Quantum Theory and Measurement* (Princeton: Princeton University Press)].
- [9] Kwiat, P. G., Waks, E., White, A. J., Appelbaum, I., and Eberhard, P. H., 1999, *Phys. Rev. A*, **60**, R773.
- [10] Bohm, D., 1951 *Quantum Theory* (Englewood Cliffs, NJ: Prentice Hall), p. 614.
- [11] Bohm, D., and Aharonov, Y., 1957, *Phys. Rev.*, **108**, 1070.
- [12] Atatüre, M., Di Giuseppe, G., Shaw, M. D., Sergienko, A. V., Saleh, B. E. A., and Teich, M. C., 2002, *Phys. Rev. A*, **66**, 023822.
- [13] Hong, C. K., Ou, Z. Y. and Mandel, L., 1987, *Phys. Rev. Lett.*, **59**, 2044.

- [14] Kwiat, P. G., Steinberg, A. M., and Chiao, R. Y., 1993, *Phys. Rev. A*, **47**, R2472.
- [15] Rarity, J. G., and Tapster, P. R., 1990, *Phys. Rev. Lett.*, **64**, 2495.
- [16] Ou, Z. Y., and Mandel, L., 1988, *Phys. Rev. Lett.*, **61**, 5; Shih, Y. H., and Alley, C. O., 1988, *Phys. Rev. Lett.*, **61**, 2921; Shih, Y. H., and Sergienko, A. V., 1994, *Phys. Lett. A*, **191**, 201; Kwiat, P. G., Mattle, K., Weinfurter, H., Zeilinger, A., Sergienko, A. V., and Shih, Y. H., 1995, *Phys. Rev. Lett.*, **75**, 4337.
- [17] Joobeur, A., Saleh, B. E. A., and Teich, M. C., 1994, *Phys. Rev. A*, **50**, 3349; Monken, C. H., Souto Ribeiro, P. H., and Pádua, S., 1998, *Phys. Rev. A*, **57**, 3123; Saleh, B. E. A., Joobeur, A., and Teich, M. C., 1998, *Phys. Rev. A*, **57**, 3991.
- [18] Atatüre, M., Di Giuseppe, G., Sergienko, A. V., Saleh, B. E. A., and Teich, M. C., 2002, *Phys. Rev. A*, **65**, 023808.
- [19] Atatüre, M., Di Giuseppe, G., Shaw, M. D., Sergienko, A. V., Saleh, B. E. A., and Teich, M. C., 2002, *Phys. Rev. A*, **66**, 023822.
- [20] Gisin, N., Ribordy, G., Tittel, W., and Zbinden, H., 2002, *Rev. mod. Phys.*, **74**, 145.
- [21] Sergienko, A. V., Atatüre, M., Walton, Z., Jaeger, G., Saleh, B. E. A., and Teich, M. C., 1999, *Phys. Rev. A*, **60**, R2622.
- [22] Jennewein, T., Simon, C., Weihs, G., Weinfurter, H., and Zeilinger, A., 2000, *Phys. Rev. Lett.*, **84**, 4729.
- [23] Tittel, W., Brendel, J., Zbinden, H., and Gisin, N., 2000, *Phys. Rev. Lett.*, **84**, 4737.
- [24] Wootters, W. K., and Zurek, W. H., 1982, *Nature*, **299**, 802.
- [25] Bennett, C. H., and Brassard, G., 1984, *Proceedings of the IEEE International Conference on Computer Systems and Signal Processing*, Bangalore, India, December 1984 p. 175.
- [26] Ekert, A. K., 1991, *Phys. Rev. Lett.*, **67**, 661.
- [27] Franson, J. D., 1991, *Phys. Rev. A*, **44**, 4552.
- [28] Dauler, E., Jaeger, G., Muller, A., Migdall, A., and Sergienko, A. V., 1999, *J. Res. NIST*, **104**, 1.
- [29] Branning, D., Migdall, A. L., and Sergienko, A. V., 2000, *Phys. Rev. A*, **62**, 063808.
- [30] Drude, P., 1890, *Ann. Phys. Chem.*, **39**, 481.
- [31] Azzam, R. M. A., and Bashara, N. M., 1977, *Ellipsometry and Polarized Light* (Amsterdam: North-Holland).
- [32] Tompkins, H. G., and McGahan, W. A., 1999, *Spectroscopic Ellipsometry and Reflectometry* (New York: Wiley).
- [33] Rothen, A., 1945, *Rev. Sci. Instrum.*, **16**, 26.
- [34] Winterbottom, A. B., 1946, *Trans. Faraday Soc.*, **42**, 487.
- [35] Mansuripur, M., 2000, *Opt. Phot. News*, **11**, 52.
- [36] Vanhellemont, J., Maes, H. E., Schaekers, M., Armigliato, A., Cerva, H., Cullis, A., de Sande, J., Dinges, H., Hallais, J., Nayar, V., Pickering, C., Stehlé, J.-L., Landuyt, J. V., Walker, C., Werner, H., and Salieri, P., 1993, *Appl. surf. Sci.*, **63**, 45.
- [37] Russev, S. C., Drolet, J., and Ducharme, D., 1998, *Appl. Opt.*, **37**, 5912.
- [38] Klyshko, D. N., 1967, *Pis'ma Zh. Eksp. Teor. Fiz.*, **6**, 490 [1967, *Sov. Phys. JETP Lett.*, **6**, 23].
- [39] Harris, S. E., Oshman, M. K., and Byer, R. L., 1967, *Phys. Rev. Lett.*, **18**, 732.
- [40] Giallrenzi, T. G., and Tang, C. L., 1968, *Phys. Rev.*, **166**, 225.
- [41] Kleinman, D. A., 1968, *Phys. Rev.*, **174**, 1027.
- [42] Abouraddy, A. F., Toussaint, K. C., Sergienko, A. V., Saleh, B. E. A., and Teich, M. C., 2001, *Opt. Lett.*, **26**, 1717.
- [43] Abouraddy, A. F., Toussaint, K. C., Sergienko, A. V., Saleh, B. E. A., and Teich, M. C., 2002, *J. opt. Soc. Am. B*, **19**, 656. Note that in equations (13)–(15), $\tan^2\psi$ should be replaced by $\tan\psi$ and $\tan\psi$ should be replaced by $(\tan\psi)^{1/2}$.
- [44] Teich, M. C., and Saleh, B. E. A., 1985, *J. opt. Soc. Am. B*, **2**, 275.
- [45] Teich, M. C., and Saleh, B. E. A., 1988, *Progr. Opt.*, **26**, 1.
- [46] Teich, M. C., and Saleh, B. E. A., 1988, *Progress in Optics*, Vol. 26, edited by E. Wolf (Amsterdam: North-Holland), chap. 1, pp. 1–104; Teich, M. C., and Saleh, B. E. A., 1990, *Phys. Today*, **43**, 26.
- [47] Kwiat, P. G., Mattle, K., Weinfurter, H., Zeilinger, A., Sergienko, A. V., and Shih, Y. H., 1995, *Phys. Rev. Lett.*, **75**, 4337.
- [48] Sergienko, A. V., Shih, Y. H., and Rubin, M. H., 1995, *J. opt. Soc. Am. B*, **12**, 859.
- [49] Fano, U., 1957, *Rev. mod. Phys.*, **29**, 74.
- [50] Abouraddy, A. F., Saleh, B. E. A., Sergienko, A. V., and Teich, M. C., 2001, *Phys. Rev. A*, **64**, 050101(R).
- [51] Zeidler, J. R., Kohles, R. B., and Bashara, N. M. 1974, *Appl. Opt.*, **13**, 1938.
- [52] Palik, E. D. (ed.), 1985, *Handbook of Optical Constants of Solids* (New York: Academic Press).
- [53] Palik, E. D. (ed.), 1995, *Handbook of Optical Constants of Solids III* (New York: Academic Press).
- [54] Huang, D., Swanson, E. A., Lin, C. P., Schuman, J. S., Stinson, W. G., Chang, W., Hee, M. R., Flotte, T., Gregory, K., Puliafito, C. A., and Fujimoto, J. G., 1991, *Science*, **254**, 2278.
- [55] Abouraddy, A. F., Nasr, M. B., Saleh, B. E. A., Sergienko, A. V., and Teich, M. C., 2002, *Phys. Rev. A*, **65**, 053817.
- [56] Campos, R. A., Saleh, B. E. A., and Teich, M. C., 1990, *Phys. Rev. A*, **42**, 4127.
- [57] Lide, D. R. (ed.), 1993, *CRC Handbook of Chemistry and Physics*, 74th edition (Boca Raton: CRC Press).